

# Dual-diode quantum-well modulator for C-band wavelength conversion and broadcasting

Hilmi Volkan Demir, Vijit A. Sabnis, Onur Fidaner,  
James S. Harris, Jr., and David A. B. Miller

*Edward L. Ginzton Laboratory, Stanford University, Stanford, California 94305*  
[volkan@stanford.edu](mailto:volkan@stanford.edu)

Jun-Fei Zheng

*Intel Strategic Technology, Intel Corporation, Santa Clara, California 95052*

**Abstract:** We present a dual-diode, InGaAsP/InP quantum-well modulator that incorporates a monolithically-integrated, InGaAs photodiode as a part of its on-chip, InP optoelectronic circuit. We theoretically show that such a dual-diode modulator allows for wavelength conversion with 10-dB RF-extinction ratio using 7 mW absorbed optical power at 10 Gb/s. We experimentally demonstrate unlimited wavelength conversion across 45 nm between 1525 nm and 1570 nm, and dual-wavelength broadcasting over 20 nm between 1530 nm and 1565 nm, spanning the entire C-band with >10dB RF-extinction ratio and using 3.1-6.7 mW absorbed optical power at 1.25 Gb/s.

©2004 Optical Society of America

**OCIS codes:** (250.3140) Integrated optoelectronic circuits; (130.3120) Integrated optics devices; (230.5590) Quantum-well devices; (230.4110) Modulators; (130.0250) Optoelectronics

---

## References and links

1. L. A. Coldren, "Widely-tunable chip-scale transmitters and wavelength converters," Integrated Photonics Research (IPR) (OSA Technical Digest, Optical Society of America, Washington, DC, 2003), pp. 6-8.
2. V. Sabnis, H.V. Demir, M. B. Yairi, J.S. Harris, Jr., D. A. B. Miller, "Observation of wavelength-converting optical switching at 2.5 GHz in a surface-normal illuminated waveguide," Proc. of Conference on Lasers and Electro-optics (LEOS), pp. 362-363, San Diego, CA, 2001.
3. S. Hoffeldt, S. Bischoff, and J. Mork, "All-optical wavelength conversion and signal regeneration using an electroabsorption modulator," J. Lightwave Technol. **18**, 1121-1127 (2000).
4. T. Otani, T. Miyazaki, S. Yamamoto, "Optical 3R regenerator using wavelength converters based on electroabsorption modulator for all-optical network applications," IEEE Photon. Tech. Lett. **12**, 431-433, (2000).
5. M. Hayashi, H. Tanaka, K. Ohara, T. Otani, M. Suzuki, "OTDM transmitter using WDM-TDM conversion with an electroabsorption wavelength converter," J. Lightwave Technol. **20**, 236-242, (2002).
6. H.V. Demir, V. A. Sabnis, O. Fidaner, J. S. Harris, Jr., D. A. B. Miller, J.-F. Zheng, N. Li, T.-C. Wu, Y.-M. Houng. "Novel optically-controlled optical switch based on intimate integration of surface-normal photodiode and waveguide electroabsorption modulator for wavelength conversion," Proc. Conference on Lasers and Electro-optics (LEOS), pp.644-645, Tuscon, AZ, 2003.
7. V. A. Sabnis, H. V. Demir, O. Fidaner, J. S. Harris, Jr., D. A. B. Miller, J.-F. Zheng, N. Li, T.-C. Wu, Y.-M. Houng, "Optically-controlled electroabsorption modulators for unconstrained wavelength conversion," Appl. Phys. Lett., 2004 (to be published).
8. H.V. Demir, V. A. Sabnis, J.-F. Zheng, O. Fidaner, J. S. Harris, Jr., D. A. B. Miller, "Novel scalable wavelength-converting crossbar," Optical Fiber Communication Conference (OFC), (Optical Society of America, Washington, D.C., 2004) paper FD5, (to be published).
9. S. Kodama, T. Ito, N. Watanabe, S. Kondo, H. Takeuchi, H. Ito, T. Ishibashi, "200 Gbit/s monolithic photodiode-electroabsorption modulator optical gate," Device Research Conference (DRC), pp. 151-152, Notre Dame, IN, 2001.
10. M. B. Yairi, H.V. Demir, and D. A. B. Miller, "Optically controlled optical gate with an optoelectronic dual diode structure: theory and experiment," Opt. Quantum Electron. **33**, 1035-1054, (2001).

11. V. A. Sabnis, H. V. Demir, O. Fidaner, J. S. Harris, Jr., D. A. B. Miller, J.-F. Zheng, N. Li, T.-C. Wu, Y.-M. Houng. "Optically-switched dual-diode electroabsorption modulators," Integrated Photonics Research (IPR) (OSA Technical Digest, Optical Society of America, Washington, DC, 2003), pp.12-14.
12. J.-F. Zheng, J. P. Hanberg, H. V. Demir, V. A. Sabnis, O. Fidaner, J. S. Harris, Jr., D. A. B. Miller, "Novel passivation and planarization in the integration of III-V semiconductor devices," Proc. of SPIE Photonics West Conference, paper 5356-9, San Jose, CA (January 24-29, 2004) (to be published).

## 1. Introduction

RF-driven electroabsorption waveguide modulators are increasingly used in commercial, high-speed optical transmitters. Their on-chip integration with edge-emitting laser diodes and semiconductor optical amplifiers along a waveguide allows low-cost, high-power, high-extinction ratio, low-chirp, high-speed transmitters [1]. Electroabsorption modulators further offer interesting network functions based on their ability to be switched optically through cross absorption modulation, for example, by field screening [2] and absorption saturation [3]. Such switching applications include all-optical wavelength conversion [2-4], optical signal regeneration [3, 4], and conversion from wavelength-division-multiplexing (WDM) to time-division-multiplexing (TDM) [5]. Despite the promising results of the previous demonstrations, the need to deliver high input signal power and/or to track input signal polarization adversely affects their potential use in optical switching and networking. Furthermore, conventional electroabsorption modulators typically exhibit wavelength-dependent optical switching, impeding their full utilization in a WDM system. For instance, conversion from a longer wavelength to a shorter one may be not as efficient as in the other direction when using cross absorption modulation. To avoid these limitations, we present a dual-diode electroabsorption waveguide modulator that incorporates an on-chip, surface-illuminated photodiode, as sketched in Fig. 1 [6, 7]. Such dual-diode modulators require low optical input power to switch with high RF-extinction ratios at data bit rates important for telecommunication. They are completely insensitive to the polarization of the optical input data streams incident on the integrated surface-normal photodiodes. They operate over a wide range of wavelengths. They provide unconstrained, bi-directional wavelength conversion and broadcasting.

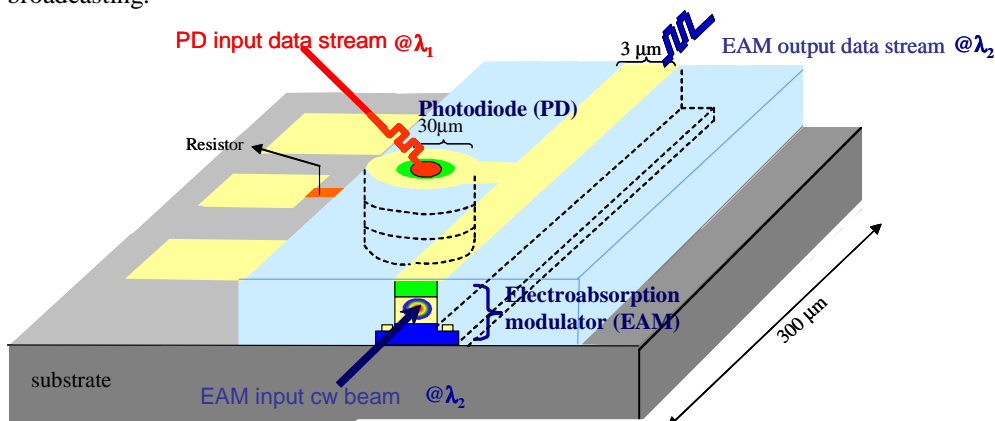


Fig. 1. A three-dimensional schematic of a dual-diode electroabsorption modulator (EAM), incorporating an on-chip photodiode (PD). The integrated optoelectronic circuit also includes a local thin film resistor.

Such dual-diode electroabsorption modulators are scalable into two-dimensional wavelength-converting crossbar switches, unlike conventional waveguide modulators [8]. They can also be engineered for ultrafast switching, for instance, through traveling-wave modulation [9] or diffusive conduction [2, 10], offering interesting TDM applications [9]. Here, for WDM applications, using a dual-diode InGaAsP/InP quantum-well modulator

directly driven by a broadband-absorbing, InGaAs photodiode, we report completely unlimited, bi-directional wavelength conversion across 45 nm between 1525 nm and 1570 nm, and multi-wavelength broadcasting over 20 nm between 1530 nm and 1565 nm, covering the entire telecommunication center (C-) band.

## 2. Device: design and implementation

Figure 2(a) shows a simplified circuit diagram of the integrated photodiode-modulator structure [6, 7]. The input signal at  $\lambda_1$  incident on the photodiode, PD, generates a photocurrent,  $I_{PD}$ , that creates a voltage drop across the resistor,  $R$ , and hence, across the electroabsorption modulator, EAM. With such optically-induced voltage swing across the modulator, the transmission through the modulator at  $\lambda_2$  is changed. Thus, the input data is bit-by-bit transferred to the output, which converts the signal wavelength from  $\lambda_1$  to  $\lambda_2$ .

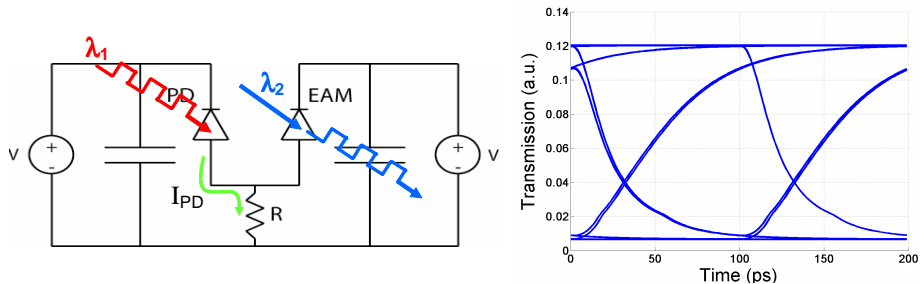


Fig. 2. (a) A simplified circuit of the integrated photodiode-modulator (PD-EAM), and (b) a simulated modulator transmission with >10dB extinction ratio at 10 Gb/s.

Our device model that includes the on-chip, integrated optoelectronic circuit and off-chip, biasing circuit predicts optical switching requiring 7 mW average absorbed optical power for 10-dB extinction ratio at 10 Gb/s. Figure 2(b) illustrates an open eye diagram of the modulator output for no-return-to-zero (NRZ) scheme produced by our simulation with a pseudo-random data sequence, and using empirical quantum-well electroabsorption. This photodiode-modulator design comprises an InGaAsP/InP quantum-well waveguide modulator with a width of 2  $\mu\text{m}$ , a length of 300  $\mu\text{m}$  and a 0.37  $\mu\text{m}$  thick *i*-region; an InGaAs photodiode with a 30  $\mu\text{m}$  x 30  $\mu\text{m}$  mesa, a 1.25  $\mu\text{m}$  thick absorbing region, and a 1.46  $\mu\text{m}$  thick *i*-region; and a local resistor of 120 Ohms.

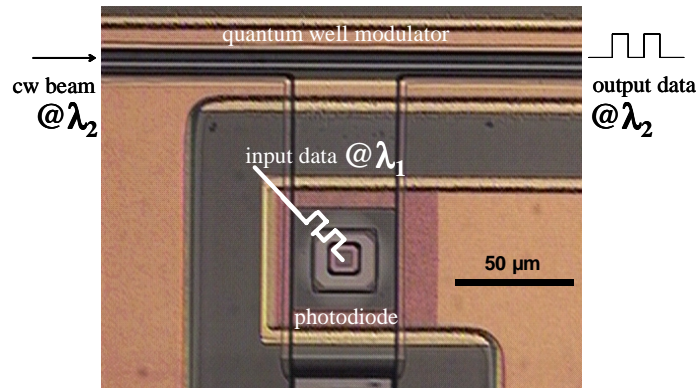


Fig. 3. A plan-view CCD microscope picture of a fabricated photodiode-modulator switch.

To study the characteristics of wavelength conversion and broadcasting, we fabricated and tested the photodiode-modulator switch shown in Fig 3. This structure consists of an InGaAsP/InP quantum-well waveguide modulator with a width of 3  $\mu\text{m}$ , a length of 300  $\mu\text{m}$  and a 0.5  $\mu\text{m}$  thick *i*-region; an InGaAs photodiode with a 30  $\mu\text{m}$  x 30  $\mu\text{m}$  mesa, a 1.25  $\mu\text{m}$

thick absorbing region, and a 1.46  $\mu\text{m}$  thick *i*-region; and an on-chip TaN thin film resistor of 650 Ohms. The fabricated device exhibits a switching bandwidth of  $\sim 1$  GHz, slightly reduced from the targeted value due to parasitic contact resistances. There are ten strain-compensated InGaAsP/InP quantum wells in the modulator with a photoluminescence peak at  $\sim 1485$  nm. The photodiode and modulator are separated only by 50  $\mu\text{m}$ . The detailed epitaxial layer designs are given both for the modulator and the photodiode in Table 1. To monolithically integrate the modulator with the photodiode, we made use of a new selective area regrowth technique [11], and a novel, self-aligning polymer planarization and passivation method [12]. Figure 4 shows cross-sectional SEM pictures across the integrated modulator and photodiode.

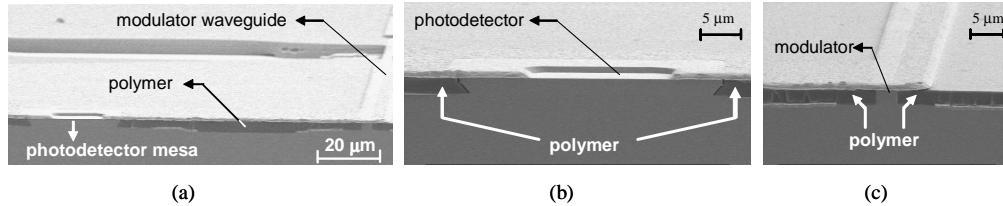


Fig. 4. SEM cross-sectional pictures across the photodiode-modulator integrated with the use of a polymer: (a) together, (b) in the vicinity of the photodiode, and (c) in the vicinity of the modulator.

Table 1. Epitaxial layers of the modulator (left) and the photodiode (right). After growing the modulator and subsequently etching its selected areas down to the 3<sup>rd</sup> layer, the photodiode is grown only on the selected areas starting from its 4<sup>th</sup> layer [11]. (u.i.d.: un-intentionally-doped)

500 Å InGaAs (Zn, $1.00 \times 10^{19}$ )		500 Å InGaAs (Zn, $1.00 \times 10^{19}$ )
10000 Å InP (Zn, $5.00 \times 10^{17}$ )		1000 Å InP (Zn, $3.00 \times 10^{18}$ )
3000 Å InP (Zn, $1.5 \times 10^{17}$ )		2300 Å InP (Zn, $5.00 \times 10^{17}$ )
1950 Å InP (u.i.d)		3000 Å InP (Zn, $1.5 \times 10^{17}$ )
200 Å 1.1Q $\text{In}_x\text{Ga}_{1-x}\text{As}_y\text{P}_{1-y}$		1500 Å InP (u.i.d)
200 Å 1.2Q $\text{In}_x\text{Ga}_{1-x}\text{As}_y\text{P}_{1-y}$		200 Å 1.1Q $\text{In}_x\text{Ga}_{1-x}\text{As}_y\text{P}_{1-y}$ (u.i.d)
200 Å 1.3Q $\text{In}_x\text{Ga}_{1-x}\text{As}_y\text{P}_{1-y}$		200 Å 1.2Q $\text{In}_x\text{Ga}_{1-x}\text{As}_y\text{P}_{1-y}$ (u.i.d)
60 Å 1.22Q $\text{In}_x\text{Ga}_{1-x}\text{As}_y\text{P}_{1-y}$	( $\times 10$ )	200 Å 1.3Q $\text{In}_x\text{Ga}_{1-x}\text{As}_y\text{P}_{1-y}$ (u.i.d)
80 Å 1.56Q $\text{In}_x\text{Ga}_{1-x}\text{As}_y\text{P}_{1-y}$		12500 Å InGaAs (u.i.d)
60 Å 1.22Q $\text{In}_x\text{Ga}_{1-x}\text{As}_y\text{P}_{1-y}$		3300 Å InP (Si, $5.0 \times 10^{17}$ )
200 Å 1.3Q $\text{In}_x\text{Ga}_{1-x}\text{As}_y\text{P}_{1-y}$		5500 Å InP (Si, $5.0 \times 10^{17}$ )
200 Å 1.2Q $\text{In}_x\text{Ga}_{1-x}\text{As}_y\text{P}_{1-y}$		200 Å 1.3Q $\text{In}_x\text{Ga}_{1-x}\text{As}_y\text{P}_{1-y}$
200 Å 1.1Q $\text{In}_x\text{Ga}_{1-x}\text{As}_y\text{P}_{1-y}$		2500 Å InP
390 Å InP (u.i.d.)		SI InP
8500 Å InP (Si, $5.0 \times 10^{17}$ )		
200 Å 1.3Q $\text{In}_x\text{Ga}_{1-x}\text{As}_y\text{P}_{1-y}$		
(Si, $3.0 \times 10^{18}$ )		
5500 Å InP (Si, $5.0 \times 10^{17}$ )		
200 Å 1.3Q $\text{In}_x\text{Ga}_{1-x}\text{As}_y\text{P}_{1-y}$		
2500 Å InP		
SI InP		

### 3. Experimental results

Figure 5(a) shows two open eye diagrams from the modulator output in (a1) NRZ and (a2) return-to-zero (RZ) schemes. These diagrams exhibited RF-extinction ratios of  $>10$  dB, typically requiring 3.1-6.7 mW absorbed optical power at 1.25 Gb/s. In both cases, the input wavelength was 1551.7 nm, and the output wavelength was 1530.0 nm. With the input beam photogenerating 2.2-4.8 mA of current, an electric field swing of 2.9-6.2 V/ $\mu\text{m}$  was optically-induced across the modulator. The photodiode handled a maximum photocurrent of 6 mA; a higher level of photocurrent caused catastrophic failure. The modulator showed a single mode operation in the C-band, and a -13dB fiber-to-fiber transmission at zero bias with a 5-

dB fiber coupling loss per facet. Figure 5(b) demonstrates a 45-nm wavelength-conversion range between the output wavelengths of 1525.0 nm in (b1) and 1570.0 nm in (b2) at 1.25 Gb/s using an optically-preamplified receiver to observe the output signal. In both cases, the input wavelength was 1551.7 nm. The wavelength-conversion range was limited due to the spectral modulation range of the quantum wells and the spectral gain range of the Erbium-doped fiber amplifiers (EDFA) used in the setup. These experiments were conducted using the setup presented in Fig. 6.

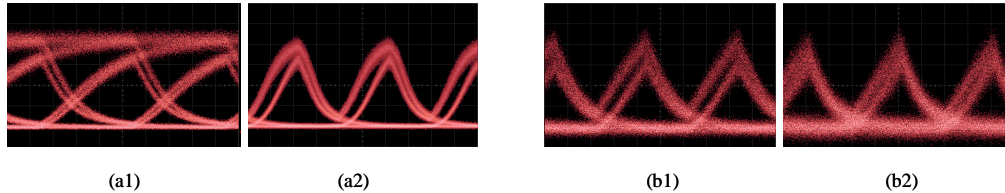


Fig. 5. (a) Optical switching in (a) NRZ and (b) RZ formats with >10dB RF-extinction ratios at 1.25 Gb/s; (b) 45-nm wavelength-conversion range between (b1) 1525.0 nm and (b2) 1570.0 nm at 1.25 Gb/s. (horizontal: 200 ps/div, vertical: 500  $\mu$ W/div)

Figure 7 represents a complete, 8x8, wavelength-conversion matrix, where 8 input and 8 output wavelengths were arbitrarily chosen within the C-band. In all cases, >10 dB RF-extinction ratio was achieved with 3.1-6.7 mW absorbed optical power at 1.25 Gb/s. The modulators were pre-biased between 4.9-10.4 V to shift the quantum-well electroabsorption for optimal modulation at each output wavelength as necessary. The waveguide setup was realigned for each wavelength, while keeping the other setup parameters such as the saturated EDFA gain fixed. The photodiode was at a fixed bias of 20 V. This wavelength-conversion matrix experimentally confirms truly unconstrained, bi-directional wavelength conversion.

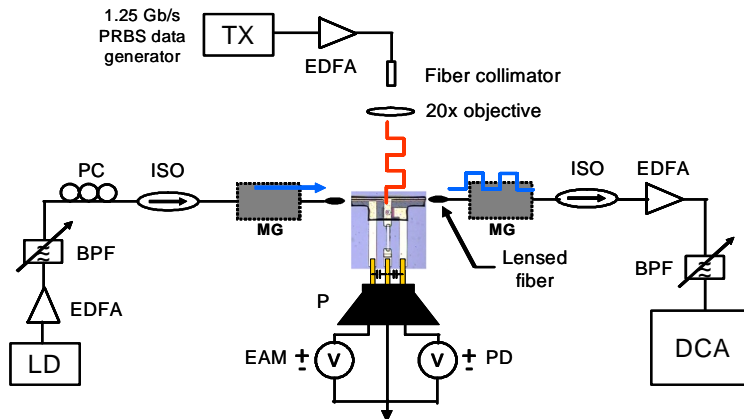


Fig. 6. Experimental setup (MG: Melles Griot 6-axis stage, DCA: digital component analyzer, TX: transmitter, LD: cw-beam laser diode, EDFA: Erbium-doped fiber amplifier, BPF: band-pass filter, PC: polarization controller, ISO: isolator, P: probe)

Figure 8 shows wavelength broadcasting over two, arbitrarily chosen, 5nm-apart channels within the C-band in (a1)-(a7). Similarly, dual-wavelength broadcasting is presented for 10 nm- and 20 nm-separated channels in the C-band, in (b1)-(b3) and (c), respectively. Applying a high enough bias (e.g., 10 V) across the modulator, the quantum-well electroabsorption is broadened over a sufficiently wide wavelength range to allow for simultaneous modulation of multiple wavelengths coupled into the same modulator.

#### 4. Conclusion

In summary, we present a dual-diode quantum-well waveguide modulator that incorporates a monolithically integrated, surface-normal photodiode. Such dual-diode modulators make polarization-insensitive optical switches that exhibit >10dB RF-extinction ratios using mW-level absorbed optical power for GHz-range switching bandwidth across a wide wavelength band. We demonstrate completely arbitrary, bi-directional wavelength conversion across 45 nm and multi-wavelength broadcasting over 20 nm, spanning the entire C-band. Our device characterization and modeling lead us to predict the feasibility of 10 Gb/s operation, by scaling down diode capacitances and thin film resistance, and minimizing parasitics.

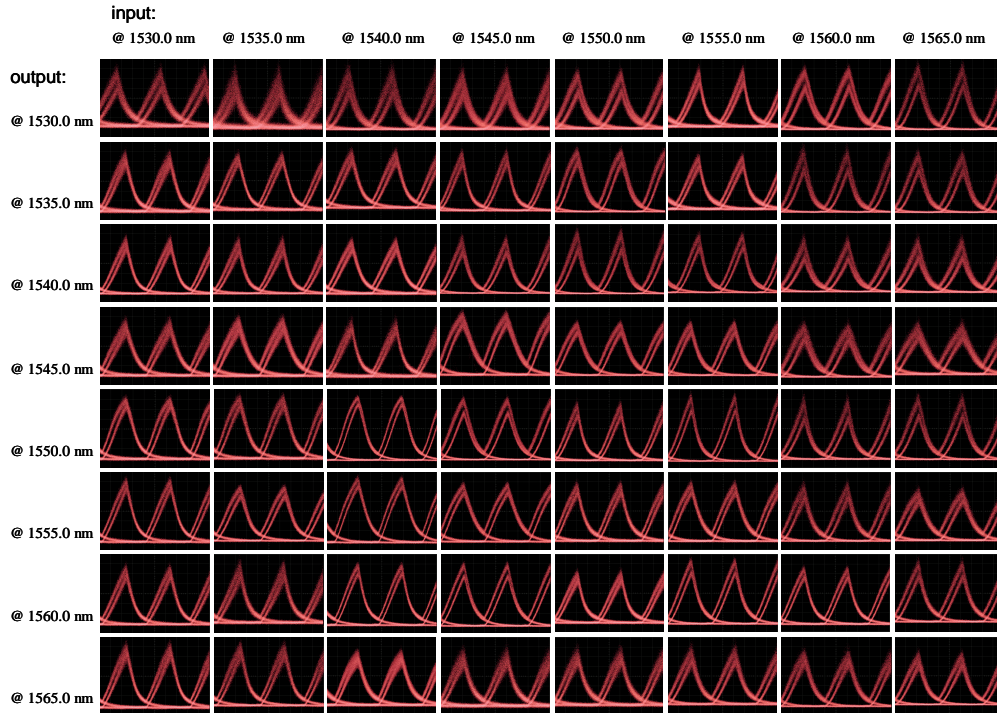


Fig. 7. 8x8 C-band wavelength conversion matrix for every possible combination of 8 input and 8 output wavelengths at 1530.0 nm, 1535.0 nm, 1540.0 nm, 1545.0 nm, 1550.0 nm, 1555.0 nm, 1560.0 nm, and 1565.0 nm. (horizontal: 200 ps/div, vertical: 448  $\mu$ W/div)

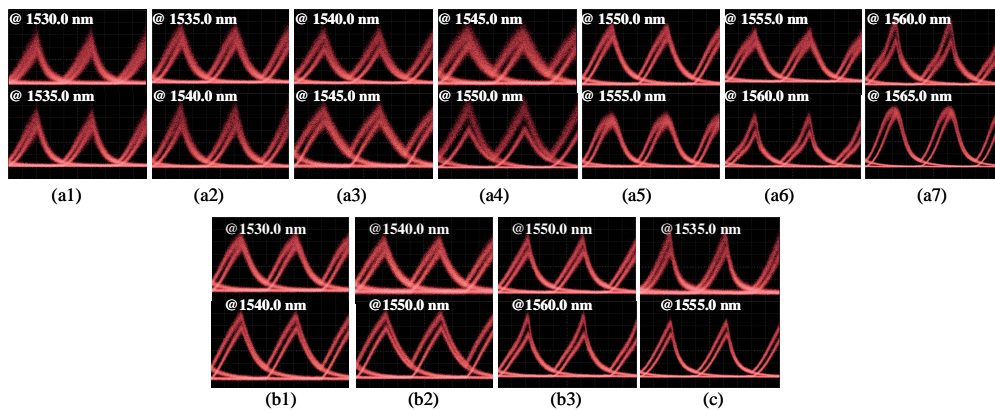


Fig. 8. C-band dual-wavelength broadcasting with channel spacings of 5 nm in (a1)-(a7), 10 nm in (b1)-(b3), and 20 nm in (c). (horizontal: 200 ps/div, vertical: 333 $\mu$ W/div)

### **Acknowledgments**

The authors acknowledge Intel Corporation for the research fund, OEpic, Inc., for the epitaxial wafer growth, and Melles Griot for the waveguide alignment setup.